Journal of Pathology Informatics 13 (2022) 100129

Contents lists available at ScienceDirect

Journal of Pathology Informatics

journal homepage: www.elsevier.com/locate/jpi

Short Communication

Automated recognition of glomerular lesions in the kidneys of mice by using deep learning

Airi Akatsuka, Yasushi Horai, Airi Akatsuka *

Syonan iPark C43 building, Muraoka-Higashi 2-26-1, Fujisawa, Kanagawa 251-8555, Japan

ARTICLE INFO

Keywords:
Digital pathology
HALO AI
Deep learning whole slide image
Automated recognition
Glomerular lesions
Pathological evaluation

ABSTRACT

Background: In recent years, digital pathology has been rapidly developing and applied throughout the world. Especially in clinical settings, it has been utilized in a variety of situations, including automated cancer diagnosis. Conversely, in non-clinical research, it has not yet been utilized as much as in clinical settings. We have been performing automated recognition of various pathological animal tissues and quantitative analysis of pathological findings, including liver and lung. In this study, we attempted to construct an artificial intelligence (AI)-based trained model that can automatedly recognize glomerular lesions in mouse kidneys that are characterized by complex structures.

Materials and methods: By using hematoxylin and eosin (HE)-stained whole slide images (WSI) from *Col4a3* KO mice as variation data, normal glomeruli and glomerular lesions were annotated, and deep learning (DL) was performed with the use of the neural network classifier DenseNet system in HALO AI. The trained model was refined by correcting the annotation of misrecognized tissue area and reperforming DL. The accuracy of the trained model was confirmed by comparing the AI-obtained results with the pathological grades evaluated by pathologists. The generality of the trained model was also confirmed by analyzing the WSI of adriamycin (ADR)-induced nephropathy mice, which is a different disease model.

Results: Glomerular lesions (including mesangial proliferation, crescent formation, and sclerosis) observed in Col4a3 KO mice and ADR mice were detected by our trained model. The number of glomerular lesions detected by our trained model were also highly correlated with that of counted by pathologists.

Conclusion: In this study, we constructed a trained model allowing us to automatedly recognize glomerular lesions in the mouse kidney with the use of the HALO AI system. The findings and insights of this study will facilitate the development of digital pathology in non-clinical research and improve the probability of success in drug discovery research.

Introduction

Digital pathology technologies, including automated image diagnosis and quantitative analysis of specific pathological findings and tissue classes, have been rapidly developing in recent years. In clinical settings, automated diagnosis of gastric cancer,[1] colorectal cancer,[2] prostate cancer,[3] and breast cancer[4] have been realized with high accuracy. In addition, automated detection and quantitative analysis of pathological findings or specific sites in the tissue are available for the diagnosis of gastropathy,[5] bone tissue,[6] and others.

In the field of renal pathology, it has become possible to automatedly recognize various structures of the kidney (e.g., tubules, tubulointerstitium, blood vessels, and glomeruli) in renal biopsy specimens,[7] glomerular lesions including glomerular sclerosis,[8,9] endocapillary proliferation, basement membrane degeneration, mesangial matrix hyperplasia, mesangial cell proliferation, and crescent.[9]

As described above, diagnostic imaging using AI and machine learning (ML) techniques has recently been developing and applied more widely in clinical practice. In contrast, in the non-clinical field, automated recognition has been attempted for tissues and cells that are relatively simple in structure, such as inflammatory regions in intestinal tissue,[10] hepatocyte hypertrophy,[11] and pathological findings in cardiomyopathy.[12] However, automated recognition, automated pathological evaluation, and quantitative analysis in more complex tissues such as the kidneys, have yet to be implemented as pathological evaluation using AI and ML techniques is still less advanced than in clinical practice. We have performed automated recognition and quantitative analysis of various pathological tissues in non-clinical animal models: recognition of bile ducts, lipid droplet sizes in the

* Corresponding author.
E-mail addresses: akatsuka.airi@ma.mt-pharma.co.jp (A. Akatsuka), horai.yasushi@md.mt-pharma.co.jp (Y. Horai), akatsuka.airi@ma.mt-pharma.co.jp (A. Akatsuka).

http://dx.doi.org/10.1016/j.jpi.2022.100129
Received 24 June 2022Received in revised form 25 July 2022Accepted 25 July 2022
Available online 28 July 2022

fatty liver, and an area of necrosis in the liver tissue; recognition of tubular degeneration and basophilic changes, hyaline casts, and glomeruli in renal tissue; identification of areas of alveolar space, fibrosis, and foamy macrophages in lung tissue; identification of areas of red pulp and white pulp, as well as of the marginal zone in the spleen; and measurement of the size of adipocytes.[13–15]

If quantitative analysis utilizing digital pathology technology can be widely used in pathological evaluation, it is expected to improve the reliability of pathological evaluation data by quantifying conventional qualitative pathological grades, visualizing them numerically, and standardizing discrepancies in the evaluation criteria that may occur among pathologists. In addition, automated pathological analysis will reduce the workload of the pathologist and enable efficient and high-quality evaluations. Thus, the development of digital pathology is expected to increase the probability of success in drug discovery research.

In this study, we attempted to automatedly recognize various glomerular lesions in the mouse renal tissue (that is composed of complex structures and a wide variety of cell types), by using the pathological image analysis software HALO AI,[16] which is aimed for use in the pathology assessment of animal disease models.

Materials and methods

Formalin-fixed, paraffin-embedded tissue samples were prepared and hematoxylin and eosin (HE)-stained histological specimens from *Col4a3* KO (129-Col4a3tm1Dec/J; 9–11-weeks-old, Charles River Laboratories Japan, Inc., bred in polycarbonate cages with γ-sterilized feed CRF1 (Oriental Yeast Co. Ltd.) and water ad libitum, ethics approvEd.) and wild-type (WT) mice were used to construct a trained model. Digital whole slide images (WSI) were acquired by virtual microscopy (Aperio AT2, Leica Biosystems, Wetzlar, Germany). By using DenseNet of the image analysis platform HALO (version 3.1; Albuquerque, NM), the images of normal glomeruli and mesangial proliferated glomeruli, crescent formed glomeruli, glomerulosclerosis, hyaline casts, blood vessels, and tubules were annotated (Fig. 1), and subjected to deep learning (DL) until convergence to a cross-entropy that was <0.1. WSI were then analyzed by the trained model, and pathologists visually confirmed the results. In the cases in which the auto-recognized regions were misrecognized, the regions were corrected or appropriately annotated, and then the DL was performed again. As described above, to construct the trained model for the automated recognition, the cycle of annotation, DL, analysis, and correction/addition of annotations was repeated. To improve the recognition accuracy, the cycle was repeated until the number of misrecognized regions was reduced to an absolute minimum, or until the analysis results did not change even when further DL was performed. The cumulative number of annotations were 785 for normal glomeruli, 409 for mesangial proliferated glomeruli, 233 for crescentic glomeruli, and 120 for glomerulosclerosis. Finally, it has taken about 10 days and 2 562 449 iterations to train the AI. The recognized glomeruli with an area of less than 1000 μm^2 were excluded from the analysis, as often they are shown not to be glomerulus or their lesions are unclear.

HE-stained pathological images of *Col4a3* KO and ADR mice were automatedly analyzed, and their glomerular lesion rates (the number of

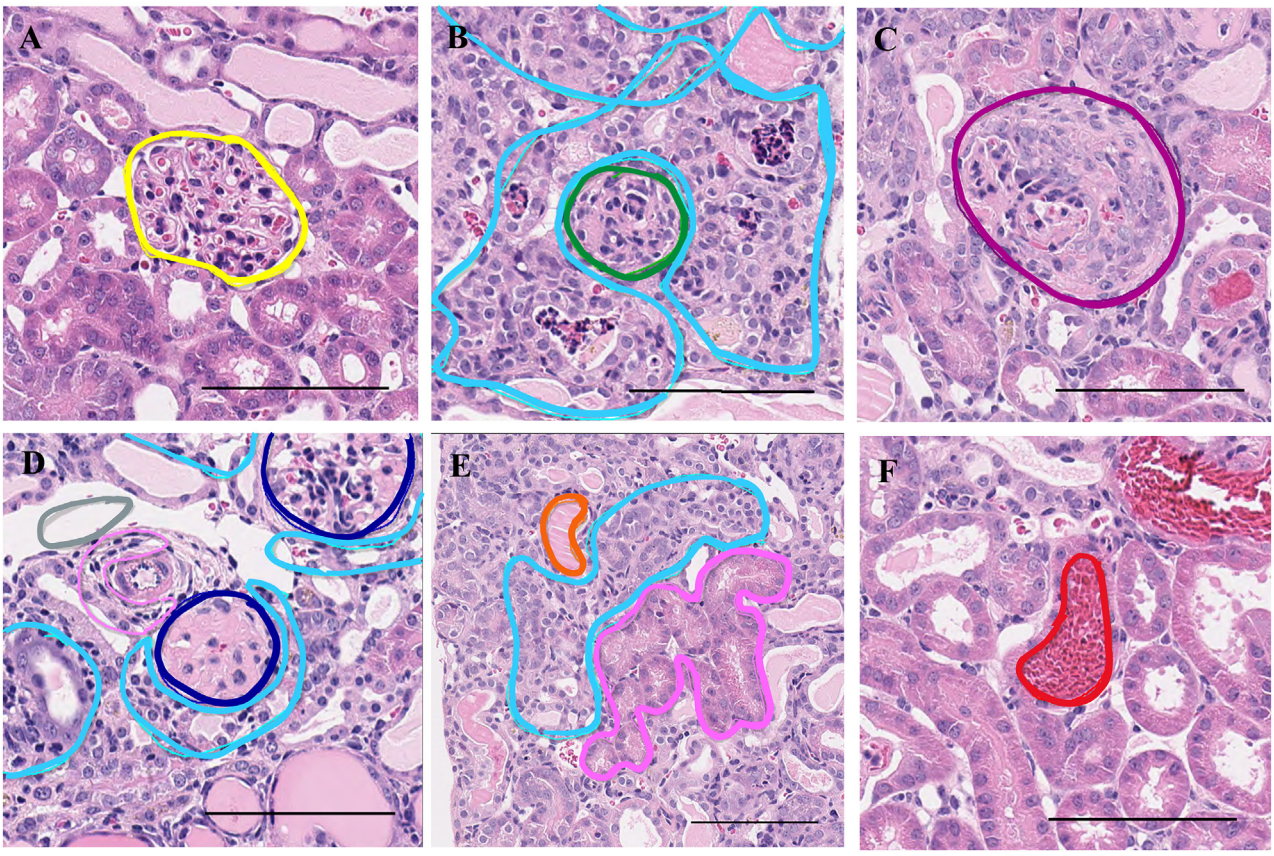

Fig. 1. Annotated images of glomeruli and tubules in pathological findings in *Col4a3* KO mice. Normal glomeruli (A, yellow), mesangial proliferated glomeruli (B, green), crescent formed glomeruli (C, purple), glomerulosclerosis (D, blue), hyaline casts (E, orange), tubules (E, pink), degenerated tubules (B, D, E, sky blue), and red blood cells (F, red) were classified by using the HALO AI system. Scale bar: 100 μm. (For interpretation of the references to colour in this figure legend, the reader is referred to the web version of this article.)

glomeruli demonstrating each type of glomerular lesion divided by the total number of glomeruli in the renal tissue of each individual mouse) were calculated. The actual glomerular lesion rates were also calculated by visually evaluating the glomeruli, and the correlation between the results of the microscopic observation grading performed by pathologists and the glomerular lesion rate recognized by HALO AI was confirmed. Furthermore, the distribution of glomeruli based on the glomerular area for each class of the assessed glomerular lesions was calculated and shown as a histogram.

Finally, to verify the generality of the trained model, we analyzed HE-stained pathology images of adriamycin (ADR)-induced nephropathy mice (12-weeks-old Balb/c, CLEA Japan, Inc., ADR was administered intravenously at a dose of 10 mg/kg, feed CRF1 and water ad libitum, ethics approved), and performed the same data analysis as in the case of the *Col4a3* KO mice.

Glomerular lesion rates were expressed as mean ± standard error, and differences between the WT and disease groups were compared by performing a Student's *t*-test with EXSUS Ver. 10.1.6.

Results

The *Col4a3* KO mouse is a disease model of the Alport syndrome. The lack of collagen type IV α3 chain causes the formation of an immature glomerular basement membrane, thereby leading to end-stage renal failure. The formation of crescent is mainly caused in the form of a glomerular lesion. In addition, the disease is characterized by intense tubulointerstitial lesions that may lead to the development of chronic kidney disease (CKD).[17]

Tubular damage (including dilation and degeneration), hyaline casts, cellular infiltration of the tubulointerstitium, and glomerular lesions (including mesangial matrix expansion, crescents, and consequent sclerosis) were observed in *Col4a3* KO mice. No lesions were observed in WT mice (Fig. 2).

To confirm the recognition accuracy of the trained model, various lesions of the glomeruli in the renal tissues of *Col4a3* KO mice were automatedly recognized, and the ratio of the number of glomeruli expressing each lesion was calculated (Fig. 3). No glomerular lesions were detected in WT mice of both sexes. In *Col4a3* KO mice, in contrast, 35.5% (±3.9%) of male and 40.1% (±4.8%) of female mice had mesangial proliferated glomeruli, 38.2% (±1.5%) of male and 31.3% (±4.0%) of female mice had crescent formed glomeruli, and 1.5% (±0.0%) of male mice had glomerulosclerosis in all glomeruli in a specimen of the kidney (Fig. 3A–C). These results were correlated with the results graded by the pathologists (Fig. 3D–F). Furthermore, the rates of each glomerular lesion recognized and quantified by HALO AI also highly correlated with the actual

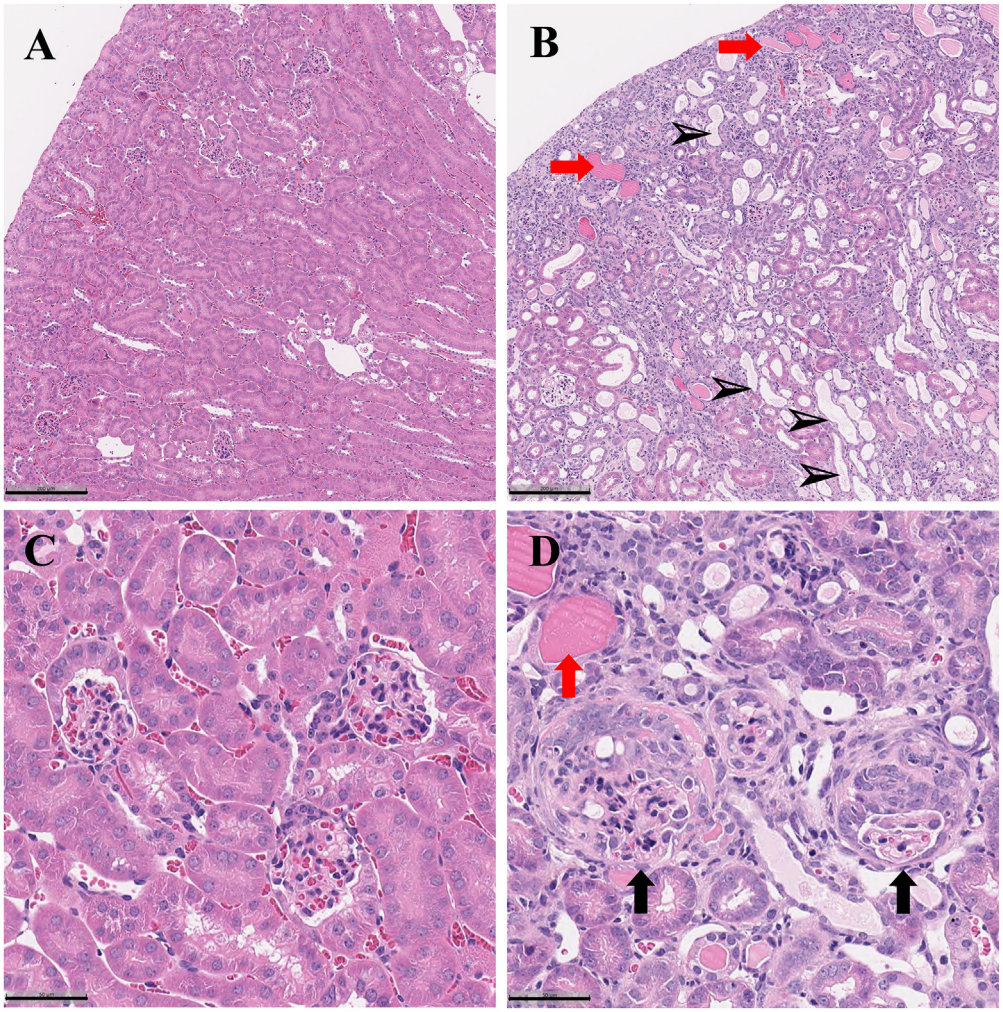

Fig. 2. Representative images of renal pathological findings in *Col4a3* KO mice. Images obtained from wild-type (WT) (A, C) and *Col4a3* KO (B, D) mice are compared. Normal glomerulus (C), hyaline casts (B, D, red arrow), dilated tubules (B, arrowhead), crescent formed glomerulus (D, arrow) are highlighted. Scale bar represents 200 μm (A, B) or 50 μm (C, D). (For interpretation of the references to colour in this figure legend, the reader is referred to the web version of this article.)

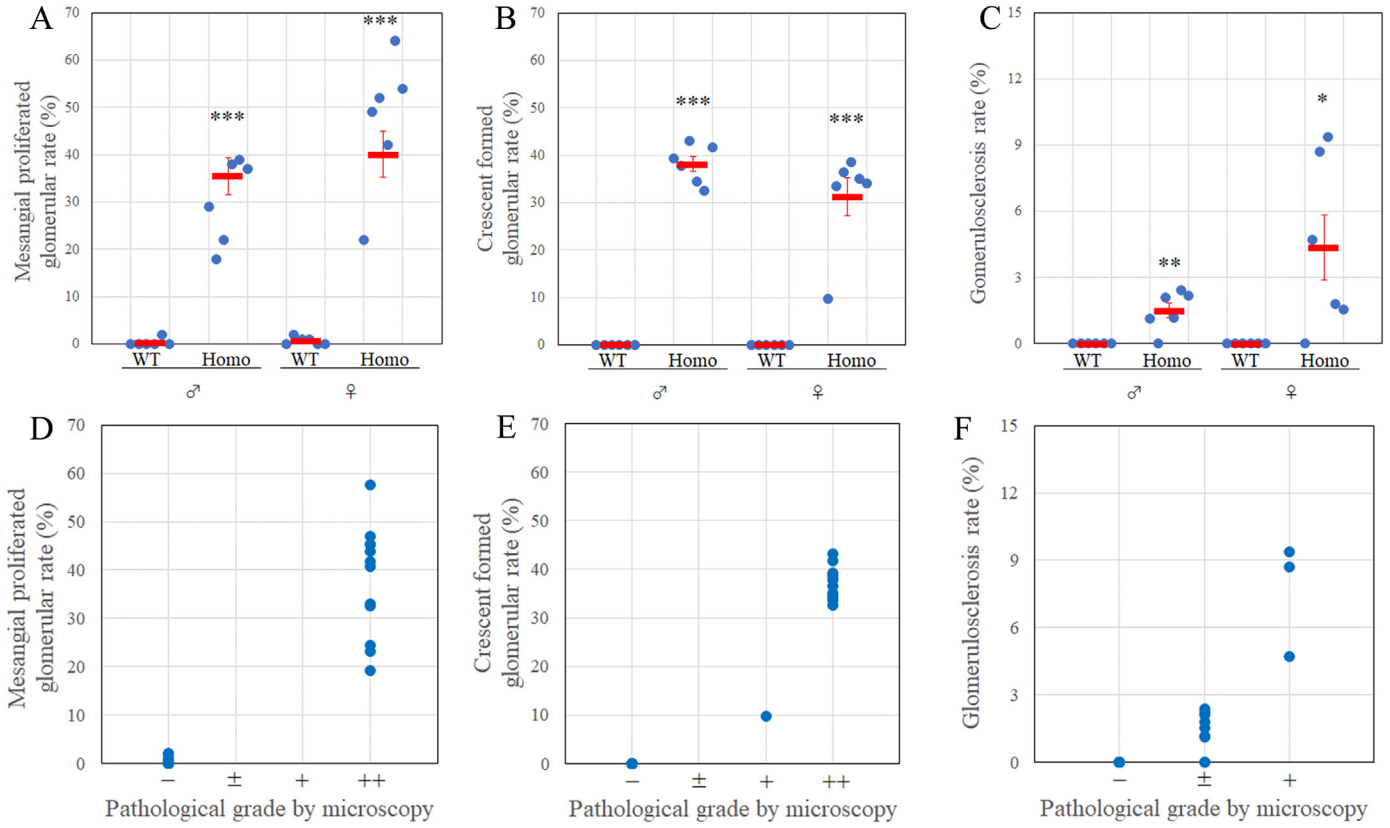

Fig. 3. The ratios of the number of glomeruli within each lesion as classified automatedly by HALO AI and their correlation to pathological grades in wild-type (WT) and *Col4a3* KO mice. Each dot represents the value of an individual mouse. Glomerular lesion rates in renal tissue specimen (A-C) are presented, where "WT" denominates wild-type mice ($n = 6$ per sex), and "Homo" denominates *Col4a3* KO mice ($n = 6$ per sex). Red bars represent the mean ± SE. $*p < 0.05$; $**p < 0.01$; $***p < 0.001$ versus WT. The correlation of the ratio of glomerular lesions for a number with pathological grades (D—F) are presented where "–" denotes no change, "±" denotes very slight changes, "+" denotes slight changes, and "++" denotes moderate changes in the pathological grade as assessed by microscopy. Mesangial proliferated glomeruli (A, D), crescent formed glomeruli (B, E), and glomerulosclerosis (C, F) rates are represented. (For interpretation of the references to colour in this figure legend, the reader is referred to the web version of this article.)

glomerular lesion rates counted by the pathologists (Fig. 4). Finally, the accuracy for the recognition of all glomeruli in this study was around 90% (data not shown).

To investigate the generality of the trained model, we subsequently analyzed another nephritis model: the ADR-induced nephropathy mice, which is a model of focal segmental glomerulosclerosis, and a well-established rodent model of CKD. The model is characterized by glomerular lesions, such as the disruption of the filtration barrier of basement membrane, followed by the development of tubulointerstitial inflammation and fibrosis.[18]

In ADR mice, tubular damage (including dilation), hyaline casts, cellular infiltration of the tubulointerstitium, and glomerular damage (including mesangial proliferation and sclerosis) were observed (Fig. 5).

The results of the automated recognition of glomerular lesions in ADR-induced nephropathy mice by using our trained model were shown (Fig. 6). No glomerular lesions were detected in WT mice. Contrastingly, in ADR mice, 25.41% (±4.17%) of mesangial proliferated glomerulus and 15.37% (±3.15%) of glomerulosclerosis were detected for total glomerular number in a specimen of the kidney (Fig. 6A, B). These quantitative results also tended to correlate with the pathological grades evaluated by pathologists (Fig. 6C, D).

The distribution according to the glomerular area for each class of glomeruli with various lesions is shown in Fig. 7. In *Col4a3* KO mice as compared to WT mice, it is indicated that the number of normal glomeruli decreased, and that of glomeruli with lesions increased. The area of the glomeruli with lesions, especially that of the crescent, was larger than the normal glomeruli respective one (Fig. 7A, B). In ADR-induced nephropathy mice, the number of normal glomeruli decreased, and that of the glomeruli with lesions increased. Moreover, the number of mesangial proliferated glomeruli with a large area increased, as compared to that of control mice (Fig. 7C, D).

Discussion

We have succeeded to automatedly recognize normal glomeruli, mesangial proliferated glomeruli, crescent formed glomeruli, and glomerulosclerosis in WSI of mouse renal specimens, by using DL. We were able to be automatedly recognize glomerular lesions in several pathological mouse models, and the results were generally and highly correlated with the conventional pathological grading results generated by microscopy.

The recognition accuracy for each class of glomeruli with lesions was finally around 90%, and some glomeruli were recognized as a mixture of

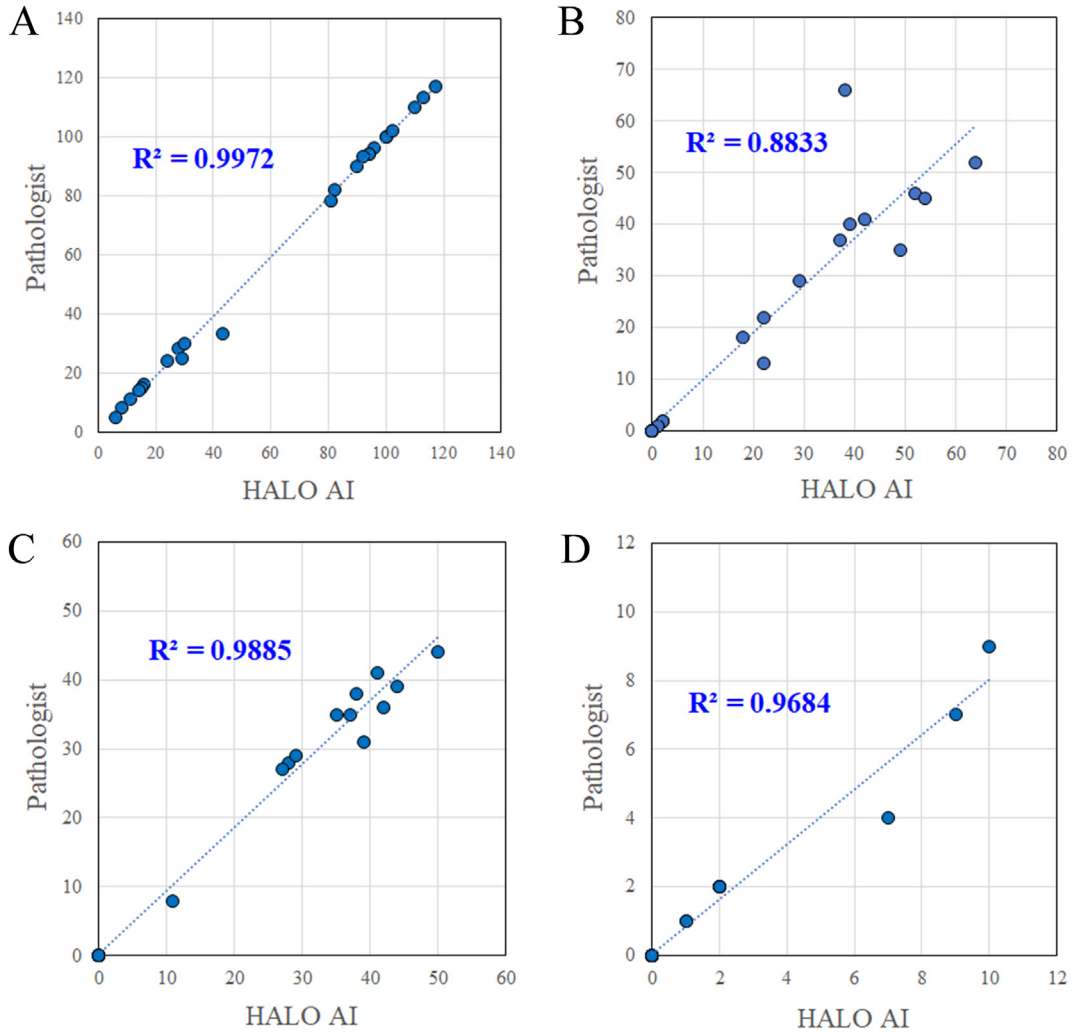

Fig. 4. The correlations between the numbers of glomerular lesions, as counted by HALO AI and pathologists in wild-type (WT) mice and *Col4a3* KO mice. Each dot represents the value obtained by an individual mouse, and the dotted line represents an approximate straight line. The numbers of normal glomeruli (A), mesangial proliferated glomeruli (B), crescent formed glomeruli (C), and glomerulosclerosis (D) are presented. Notes: R^2 stands for the correlation coefficient; WT ($n = 12$) and *Col4a3* KO ($n = 12$) mice are examined.

multiple lesions. To recognize and analyze these lesions in a fully automated manner, it is necessary to further improve the recognition accuracy. When constructing a trained model by using DL for automated recognition, the amount of image data to be trained and the number of the patterns of these pathological findings greatly affect the recognition accuracy.[19,20] In this respect, the number of annotated glomeruloscleroses was smaller than that of other classes of glomeruli; as a result, the training of the AI for glomerulosclerosis may be insufficient. To refine the trained model, it needs to be trained by more tissue image data with glomerulosclerosis. For the aspect of versatility, it is necessary to verify whether the trained model can be applied to the tissues of other animals such those of rats and humans, although we have constructed the trained model that automatedly recognized the glomerular lesions of mice in this study. In human renal pathology, it has been already attempted to automatically recognize glomerular lesions.[9] One of the problems in recognizing and analyzing tissue classes and pathological findings by using AI/DL is the difficulty in validating the trained model. Even when a commercial system like HALO AI is used, the quality of automated recognition will vary depending on the variation and number of image data used for training, the facility, and the pathologist. The criteria for standardizing these differences have not yet been established, but will be defined with the development of image analysis research using AI in the future.

In this study, it was possible to quantify the area of each glomerulus by automatedly recognizing the glomerulus through the use of HALO AI. Therefore, we could express the glomerular size for each glomerular lesion class as a histogram. In nephritis models, abnormal glomeruli appear as the disease progresses.[17,18] The number of normal glomeruli decreased, and that of glomeruli with lesions increased in the nephritis model. Furthermore, most of the glomeruli with lesions had a larger area, which is considered to be due to the proliferation of lesion components such as the mesangium and the crescent. This is a new insight for the quantification of the glomerular size that cannot be obtained by qualitative evaluation.

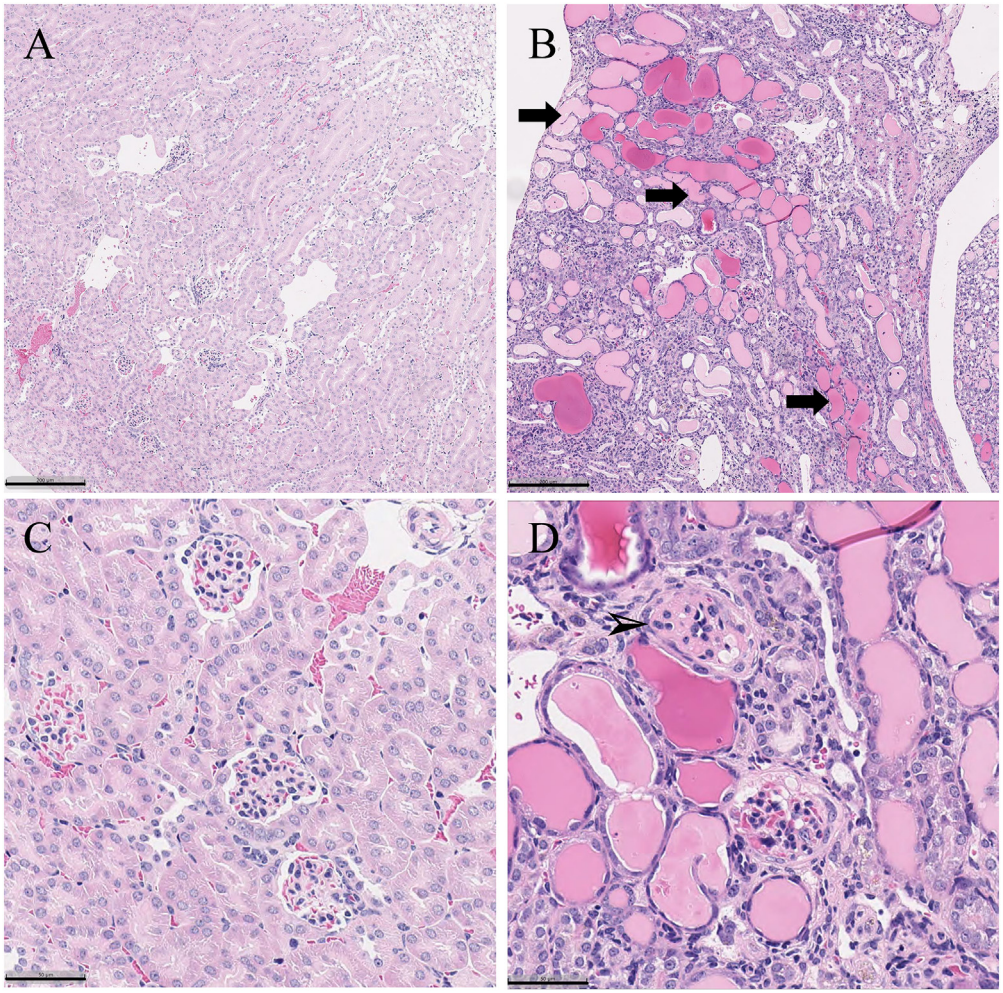

Fig. 5. Representative images of renal pathological findings of adriamycin (ADR) mice. Control mice (A, C) and ADR mice (B, D) were examined. Normal glomerulus (C), hyaline casts and dilated tubules (B), as well as glomerulosclerosis (D, arrowhead) are presented. Scale bars represent 200 μm (A, B) or 50 μm (C, D).

Thus, in addition to the recognition of the glomerular lesion, the quantitative analysis of the size will enable a more detailed investigation of the disease severity and of the effects of drugs.

As far as the pathological evaluation is concerned, the AI-based tissue recognition and quantitative analysis have the potential to detect subtle differences and trends in lesions that cannot be detected by conventional human observation. Quantitative analysis of pathological images by using HALO AI and other AI/DL technology-based systems (such as the trained model we have constructed specifically for the automated recognition of glomerular lesions), makes it possible to instantly evaluate and quantify all glomeruli on a section of renal tissue. In other words, compared to the conventional qualitative pathological evaluation undertaken by microscopy, it enables a more efficient and accurate evaluation that does not depend on the skill of the pathologist.

We intend to develop a trained model that automatedly recognizes not only glomerular lesions, but also tubular damage and inflammatory cell infiltration, and to eventually establish an automated recognition trained model that can be applied to all non-clinical nephropathy models in the future.

The experience and the know-how gained by constructing trained models for the automated recognition of pathological findings in renal tissues (which have complex structures) can be greatly applied to the automated recognition and quantitative analysis of pathological findings in other organs. This is expected to lead to the spread of digital pathology in non-clinical research, and to the enrichment of pathological evaluation data as well as to the improvement of the data reliability.

Conclusion

We have constructed the trained model to automatedly detect glomerular lesions in the mouse kidney. As we refine the trained model to be available for the analysis of all non-clinical nephropathy models, the experience and know-how gained will be highly applicable to the quantitative analysis of various tissues in the future.

The dissemination and the development of digital pathology technologies are highly expected to solve the problems encountered in conventional visual pathological evaluation, and will contribute to the improvement of the probability of success in drug discovery research.

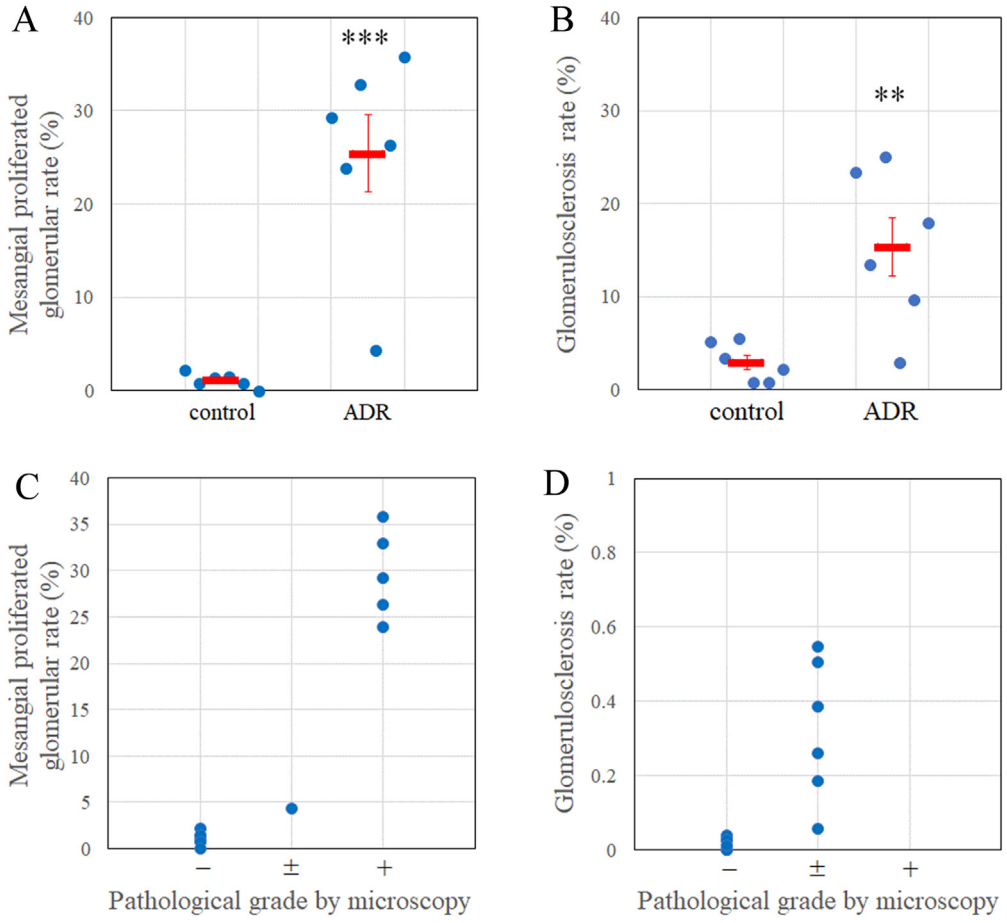

Fig. 6. The ratio of the number of glomeruli within each lesion that is classified automatedly by HALO AI, and the correlation of this ratio to the pathological grades in wild-type (WT) and adriamycin (ADR) mice. Each dot represents the value corresponding to an individual mouse. Glomerular lesion rates in renal tissue specimens are presented (A, B). Red bars represent the mean ± SE. $**p < 0.01$; $***p < 0.001$ versus control. Correlation of the ratio of glomerular lesions with pathological grades (C, D), where "–" denotes no change, "±" denotes very slight changes, and "+" denotes slight changes in the pathological grade as assessed by microscopy. The mesangial proliferated glomerular lesion (C) and the glomerulosclerosis (D) rates are examined. (For interpretation of the references to colour in this figure legend, the reader is referred to the web version of this article.)

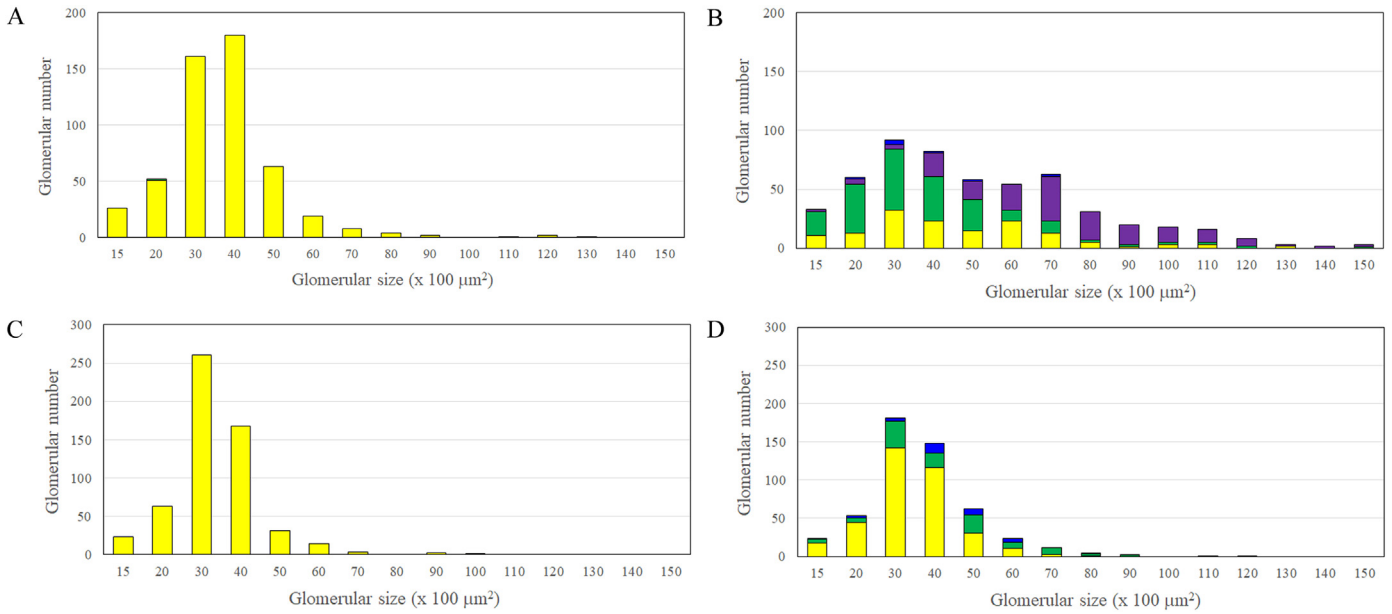

Fig. 7. Histogram of the glomerular area for each class of glomeruli, as calculated by HALO AI for wild-type (WT) (A) and *Col4a3* KO (B), control (C) and adriamycin (ADR) (D) mice. The numbers representing normal glomeruli (yellow), mesangial proliferated glomeruli (green), crescent formed glomeruli (purple), and glomerulosclerosis (blue) are highlighted. (For interpretation of the references to colour in this figure legend, the reader is referred to the web version of this article.)

Financial support and sponsorship

Not applicable.

Conflicts of interest

There are no conflicts of interest.

Acknowledgments

We would like to acknowledge all researchers in Mitsubishi Tanabe Pharma Corporation who have offered tissue specimens and supported our study.

References

1. Yoshida H, Shimazu T, Kiyuna T, et al. Automated histological classification of whole-slide images of gastric biopsy specimens. Gastric Cancer 2018;21(2):249–257. https://doi.org/10.1007/s10120-017-0731-8.
2. Yoshida H, Yamashita Y, Shimazu T, et al. Automated histological classification of whole slide images of colorectal biopsy specimens. Oncotarget 2017;8(53):90719–90729. https://doi.org/10.18632/oncotarget.21819.
3. Yamamoto Y, Offord CP, Kimura G, et al. Tumour and immune cell dynamics explain the PSA bounce after prostate cancer brachytherapy. Br J Cancer 2016;115(2):195–202. https://doi.org/10.1038/bjc.2016.171.
4. Veta M, Kornegoor R, Huisman A, et al. Prognostic value of automatically extracted nuclear morphometric features in whole slide images of male breast cancer. Mod Pathol 2012;25(12):1559–1565. https://doi.org/10.1038/modpathol.2012.126.
5. Martin DR, Hanson JA, Gullapalli RR, Schultz FA, Sethi A, Clark DP. A deep learning convolutional neural network can recognize common patterns of injury in gastric pathology. Arch Pathol Lab Med 2020;144(3):370–378. https://doi.org/10.5858/arpa.2019-0004-OA.[Epub 2019 Jun 27].
6. Hagiya AS, Etman A, Siddiqi IN, et al. Digital image analysis agrees with visual estimates of adult bone marrow trephine biopsy cellularity. Int J Lab Hematol 2018;40(2):209–214. https://doi.org/10.1111/ijlh.12768.
7. Hermsen M, de Bel T, den Boer M, et al. Deep learning-based histopathologic assessment of kidney tissue. J Am Soc Nephrol 2019;30(10):1968–1979. https://doi.org/10.1681/ASN.2019020144.
8. Ginley B, Lutnick B, Jen KY, et al. Computational segmentation and classification of diabetic glomerulosclerosis. J Am Soc Nephrol 2019;30(10):1953–1967. https://doi.org/10.1681/ASN.2018121259.
9. Uchino E, Suzuki K, Sato N, et al. Classification of glomerular pathological findings using deep learningand nephrologist–AI collective intelligence approach. Int J Med Inform 2020;141, 104231. https://doi.org/10.1016/j.ijmedinf.2020.104231.
10. Bédard A, Westerling-Bui T, Zuraw A. Proof of concept for a deep learning algorithm for identification and quantification of key microscopic features in the murine model of DSS-induced colitis. Toxicol Pathol 2021;49(4):897–904. https://doi.org/10.1177/0192623320987804.
11. Pischon H, Mason D, Lawrenz B, et al. Artificial intelligence in toxicologic pathology: quantitative evaluation of compound-induced hepatocellular hypertrophy in rats. Toxicol Pathol 2022;50(1):23–34. https://doi.org/10.1177/0192623320983244.
12. Tokarz DA, Steinbach TJ, Lokhande A, et al. Using artificial intelligence to detect, classify, and objectively score severity of rodent cardiomyopathy. Toxicol Pathol 2021;49(4):888–896. https://doi.org/10.1177/0192623320972614.
13. Horai Y, Kakimoto T, Takemoto K, Tanaka M. Quantitative analysis of histopathological findings using image processing software. J Toxicol Pathol 2017;30(4):351–358. https://doi.org/10.1293/tox.2017-0031.
14. Horai Y, Mizukawa M, Nishina H, et al. Quantification of histopathological findings using a novel image analysis platform. J Toxicol Pathol 2019;32(4):319–327. https://doi.org/10.1293/tox.2019-0022.
15. Horai Y, Akatsuka A, Mizukawa M, et al. Current status and prospects for quantitative analysis of digital image of pathological specimen using image processing software including artificial intelligence. Translat Regulat Sci 2020;2(3):72–79. https://doi.org/10.33611/trs.2020-014.
16. HALO. AI–Indica Labs. http://www.indicalab.com/halo-ai/.
17. Andrews KL, Mudd JL, Li C, Miner JH. Quantitative trait loci influence renal disease progression in a mouse model of Alport syndrome. Am J Pathol 2002;160(2):721–730. https://doi.org/10.1016/S0002-9440(10)64892-4.
18. Lee VW, Harris DC. Adriamycin nephropathy: a model of focal segmental glomerulosclerosis. Nephrology (Carlton) 2011;16(1):30–38. https://doi.org/10.1111/j.1440-1797.2010.01383.x.
19. Karimi D, Nir G, Fazli L, et al. Deep learning-based Gleason grading of prostate cancer from histopathology images—role of multiscale decision aggregation and data augmentation. IEEE J Biomed and Health Inform 2020;24(5):1413–1425. https://doi.org/10.1109/JBHI.2019.2944643.
20. Chlap P, Min H, Vandenberg N, Dowling J, Holloway L, Haworth A. A review of medical image data augmentation techniques for deep learning applications. J Med Imaging Radiat Oncol 2021;65(5):545–563. https://doi.org/10.1111/1754-9485.13261.